Excess C/H in Protoplanetary Disk Gas from Icy Pebble Drift Across the CO Snowline

Ke Zhang[1], Arthur D. Bosman, and Edwin A. Bergin
Department of Astronomy, University of Michigan, 323 West Hall, 1085 South University Avenue, Ann Arbor, MI 48109, USA; kezhang@umich.edu
Received 2020 January 20; revised 2020 February 17; accepted 2020 February 18; published 2020 March 3

Abstract

The atmospheric composition of giant planets carries the information of their formation history. Superstellar C/H ratios are seen in atmospheres of Jupiter, Saturn, and various giant exoplanets. Also, giant exoplanets show a wide range of C/O ratio. To explain these ratios, one hypothesis is that protoplanets accrete carbon-enriched gas when a large number of icy pebbles drift across the CO snowline. Here we report the first direct evidence of an elevated C/H ratio in disk gas. We use two thermo-chemical codes to model the $^{13}C^{18}O$, $C^{17}O$, and $C^{18}O$ $(2-1)$ line spectra of the HD 163296 disk. We show that the gas inside the CO snowline ($\sim$70 au) has a C/H ratio that is 1–2 times higher than the stellar value. This ratio exceeds the expected value substantially, as only 25%–60% of the carbon should be in gas at these radii. Although we cannot rule out the case of a normal C/H ratio inside 70 au, the most probable solution is an elevated C/H ratio that is 2–8 times higher than the expectation. Our model also shows that the gas outside 70 au has a C/H ratio that is $0.1\times$ the stellar value. This picture of enriched C/H gas at the inner region and depleted gas at the outer region is consistent with numerical simulations of icy pebble growth and drift in protoplanetary disks. Our results demonstrate that the large-scale drift of icy pebble can occur in disks and may significantly change the disk gas composition for planet formation.

Unified Astronomy Thesaurus concepts: Planet formation (1241); Exoplanet atmospheres (487); Astrochemistry (75); Protoplanetary disks (1300)

1. Introduction

The atmospheric compositions of giant planets carry information of their formation and evolution history (Madhusudhan 2019). Beyond hydrogen, carbon and oxygen are the two most measurable elements in planetary atmospheres, because they are highly abundant and the C/O ratio has large effects on the atmospheric chemistry of giant planets (Fortney et al. 2008; Moses et al. 2013). In the solar system, the C/H ratio in the atmospheres of Jupiter and Saturn appears to be enhanced by a factor of a few compared to the solar value (Owen et al. 1999; Atreya et al. 2005). Beyond the solar system, superstellar C/H ratios have been reported in atmospheres of several gas giant exoplanets (Madhusudhan & Seager 2011; Lee et al. 2013; Lavie et al. 2017). Current studies show that atmospheres of gas giant exoplanets have a wide range of measured C/O ratios (Madhusudhan 2012; Lee et al. 2013; Moses et al. 2013; Brogi et al. 2014; Line et al. 2014); however, there is a preponderance of superstellar C/O ratios, albeit with large uncertainties (Brewer et al. 2017).

These C/H and C/O measurements offer important constraints to test planet formation models (Madhusudhan 2012; Cridland et al. 2019). In the core-accretion formation scenario, the atmospheric composition of a giant planet is initially set by the composition of the gas within the natal disk (Pollack et al. 1996). For a *static* disk, the C/H ratio in the disk gas is expected to be always substellar as 25%–75% of the carbon is in refractory materials (Pollack et al. 1994; Mishra & Li 2015). The sublimation/destruction temperature of the carbonaceous refractory grains is at least >350 K (Gail & Trieloff 2017), which lies interior 1 au in protoplanetary disks (Tilling et al. 2012). Therefore, for the majority of the disk the gas phase C/H ratio starts at a substellar ratio and decrementally decreases with distance from the star, as various

carbon carriers subsequently freeze-out beyond their snowlines (Öberg et al. 2011b; Cridland et al. 2016; Eistrup et al. 2016). Therefore, a superstellar C/H ratio in planetary atmospheres is usually attributed to contamination of planetesimals or mixing with planetary core materials (Owen et al. 1999).

However, contamination or mixing from solids cannot explain superstellar C/O ratios seen in various exoplanets. This is because solids are more enriched by oxygen than carbon. A possible solution is that the protoplanet accretes gas with an elevated C/H ratio that is enriched by CO ice sublimation from a large amount of icy pebble drifting into the CO snowline (Öberg & Bergin 2016; Booth et al. 2017). In fact, numerical simulations of the formation and drifting of pebbles in disks have long predicted elevated C/H or O/H ratios in the gas inside snowlines (e.g., Cuzzi & Zahnle 2004; Ciesla & Cuzzi 2006; Stammler et al. 2017; Krijt et al. 2018). However, no previous observation was able to confirm the existence of C/H enriched gas in protoplanetary disks.

The HD 163296 system presents a unique target to study the spatial distribution of C/H ratio in a protostar-disk system. The C/H ratio of its stellar photosphere has been measured to be $1.5^{+1.2}_{-0.7} \times 10^{-4}$ (Folsom et al. 2012; Jermyn & Kama 2018). The total hydrogen mass of the disk is constrained by the upper limit of HD $(1-0)$ line flux (Kama et al. 2020). CO is one of the main carriers of carbon in protoplanetary disks and is expected to taken 25%–60% of total stellar carbon budget (Öberg et al. 2011b). Here we use multiple CO isotopologue $J = 2-1$ line spectra to constrain the carbon budget in the disk.

2. Observations

The observations were carried out with the NOEMA interferometer on 2019 March 9 and 20. The total on-source integration time was 3.7 hr. The observations used the wideband correlator PolyFix that has an instantaneous dual-polarization coverage of 15.5 GHz bandwidth at a fixed

---

[1] Hubble Fellow.

Table 1
Line Fluxes: Data versus Models

Line	Obs (Jy km s^{-1})	RAC2D Models				DALI Models			
		R1	R2	R3	R4	D1	D2	D3	R4
$^{13}C^{18}O$ (2−1)	0.37 ± 0.03	1.29	0.16	0.51	0.44	1.18	0.15	0.36	0.29
$C^{17}O$ (2−1)	3.36 ± 0.03	11.27	2.59	3.67	3.56	12.01	2.83	3.24	3.13
$C^{18}O$ (2−1)	6.34 ± 0.04	18.64	5.98	7.50	7.38	19.19	5.88	6.33	6.20
HD(1−0)	⩽67	108				67			

resolution of 2000 kHz. In addition, higher spectral resolution chunks were set at the line centers of $C^{18}O$, $C^{17}O$, and $^{13}C^{18}O$ (2−1) with a resolution of 65 kHz. The baseline lengths were between 24 and 368 m. Nearby quasars (1730–130 and 1830–210) were observed between science targets to calibrate the complex antenna gains. The absolute flux calibrator was MWC 349. Data calibration and imaging were done using the GILDAS software. We re-binned data to a channel width of 0.5 km s^{-1} to enhance signal-to-noise ratios. After a uniform weighting, the synthesized beam is 5″3 × 1″5 with a noise level of 8 mJy beam^{-1}. The absolute flux uncertainty is expected to be 15%–20% and the 1.3 mm continuum flux is consistent with literature values within 15%.

All isotopologue CO lines were detected. The integrated line fluxes are listed in Table 1. Line fluxes were integrated from greater than 3σ region between 0 and 12 km s^{-1}, except for the weakest $^{13}C^{18}O$ line. The $^{13}C^{18}O$ line flux was integrated using the $C^{17}O$ line $>3\sigma$ region as a mask.

3. Methods

We match the observed CO line spectra with thermo-chemical models to constrain the spatial distribution of the C/H ratio in the HD 163296 disk. To make a robust constraint, we employ two thermo-chemical codes, RAC2D and DALI, which were developed independently (Bruderer et al. 2012; Bruderer 2013; Du & Bergin 2014). Both have been used in molecular line studies of protoplanetary disks (e.g., Bergin et al. 2016; Bosman et al. 2018; Zhang et al. 2019).

3.1. Common Setups of both Codes

We employ the gas and density structures from Isella et al. (2016). The model contains two populations of grains, a population of small grains following the gas, ranging from 0.005 to 1 μm, and a second population of large grains, ranging from 0.005 to 1000 μm. The total disk mass is 0.14 $M_{\odot}$, assuming a gas-to-dust ratio of 100.

The chemical structure is computed by starting with an interstellar medium (ISM) level of elemental abundances across the whole disk[2] and then letting the chemistry and gas temperature self-consistently evolve for 1 Myr. The initial C/H abundance is set to an ISM ratio of 1.4×10^{-4}, with all carbon in CO gas. Chemical processes can turn CO into other carbon species and the efficiency is sensitive to the ionization rate in the disk, especially the cosmic-ray rate (Bosman et al. 2018; Schwarz et al. 2018). We use a cosmic-ray rate of 1.36×10^{-18} s^{-1}; this is consistent with a reduced rate through the influence of stellar winds (Cleeves et al. 2013). After 1 Myr, most of the carbon is still in CO and only less than 10% of carbon has been processed into other carbon species.

3.2. Thermo-chemical Set 1: RAC2D Models

For the first set of models, we start with the RAC2D model of the HD 163296 disk by Zhang et al. (2019). This baseline model matches the spectral energy distribution (SED) of the HD 163296 system. It has a mid-plane CO snowline at 70 au, which is consistent with earlier constraints on the CO snowline location from spatially resolved images of $C^{18}O$ and N_2H^+ lines (Qi et al. 2015).

Previous studies have reported that the CO-to-H abundance in the HD 163296 may be lower than the ISM value of 1.4×10^{-4} (Rosenfeld et al. 2013; Williams & Best 2014). Furthermore, Zhang et al. (2019) showed that the spatially resolved $C^{18}O$ (2−1) images could not be reproduced by uniformly reducing the CO abundance across the whole disk. Here, we use the following four sets of models.

1. R1: the CO gas abundance structure from the baseline RAC2D model, where the C/H abundance is 1.4×10^{-4} across the whole disk.
2. R2: we reduce the baseline CO abundance structure by a factor of 10, i.e., a C/H abundance of 1.4×10^{-5} across the whole disk.
3. R3: we use the radial-dependent CO depletion profile derived by Zhang et al. (2019), which is required to reproduce spatially resolved $C^{18}O$ (2−1) line images. The most prominent feature of the profile is that the C/H abundance rapidly increases from $\sim0.1 \times$ ISM outside the CO snowline to $2 \times$ ISM value inside the snowline.
4. R4: the same as R3, except that the C/H abundance is the ISM value inside the mid-plane CO snowline.

The detailed profiles are shown in Figure 1. We then generate model spectra of CO isotopologue lines using the ray-tracing module of the RAC2D code. The isotopologue abundance ratios are set to the local ISM CO abundance ratios of $^{18}O/^{17}O = 3.6$, $^{12}C/^{18}C = 557$, and $^{12}C/^{13}C = 69$ (Wilson 1999).

3.3. Thermo-chemical Set 2: DALI Models

Similar to RAC2D models, we vary the CO abundance structure from a baseline DALI model to compare with observations. The four sets of models are: (D1) baseline model, with a C/H ratio of 1.35×10^{-4}; (D2) all CO abundance depleted by a factor of 10; (D3) at radii larger than the mid-plane CO ice line ($T_{\mathrm{mid}} < 21$ K) the CO abundance is dropped by a factor of 10, and in the region within the CO ice line, the CO abundance is enhanced by a factor of two; (D4) the same as D3, except the C/H inside the snowline is an ISM ratio.
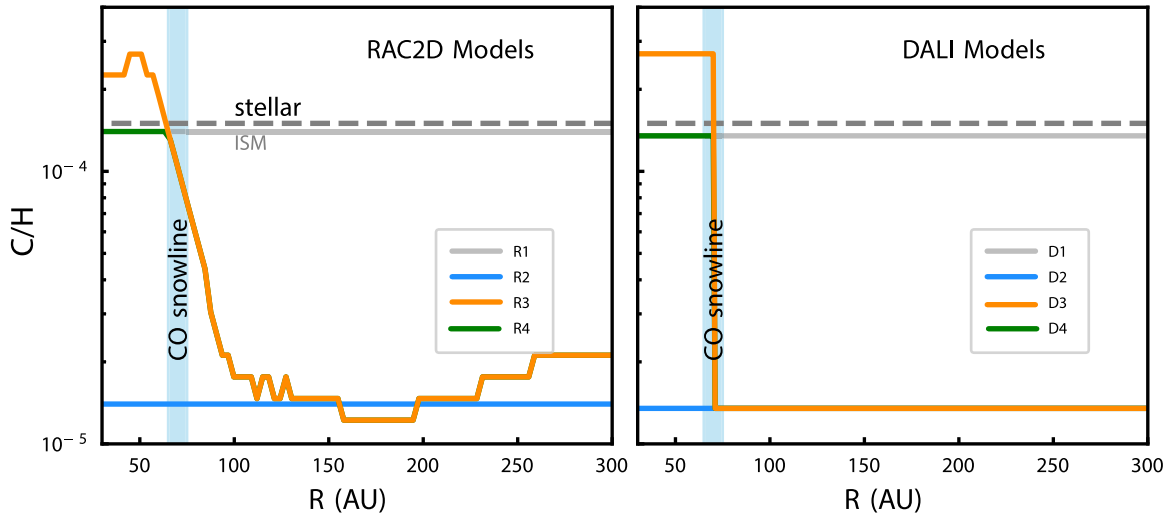
---

[2] Please see elemental abundances in the Table 1 of Du & Bergin (2014).

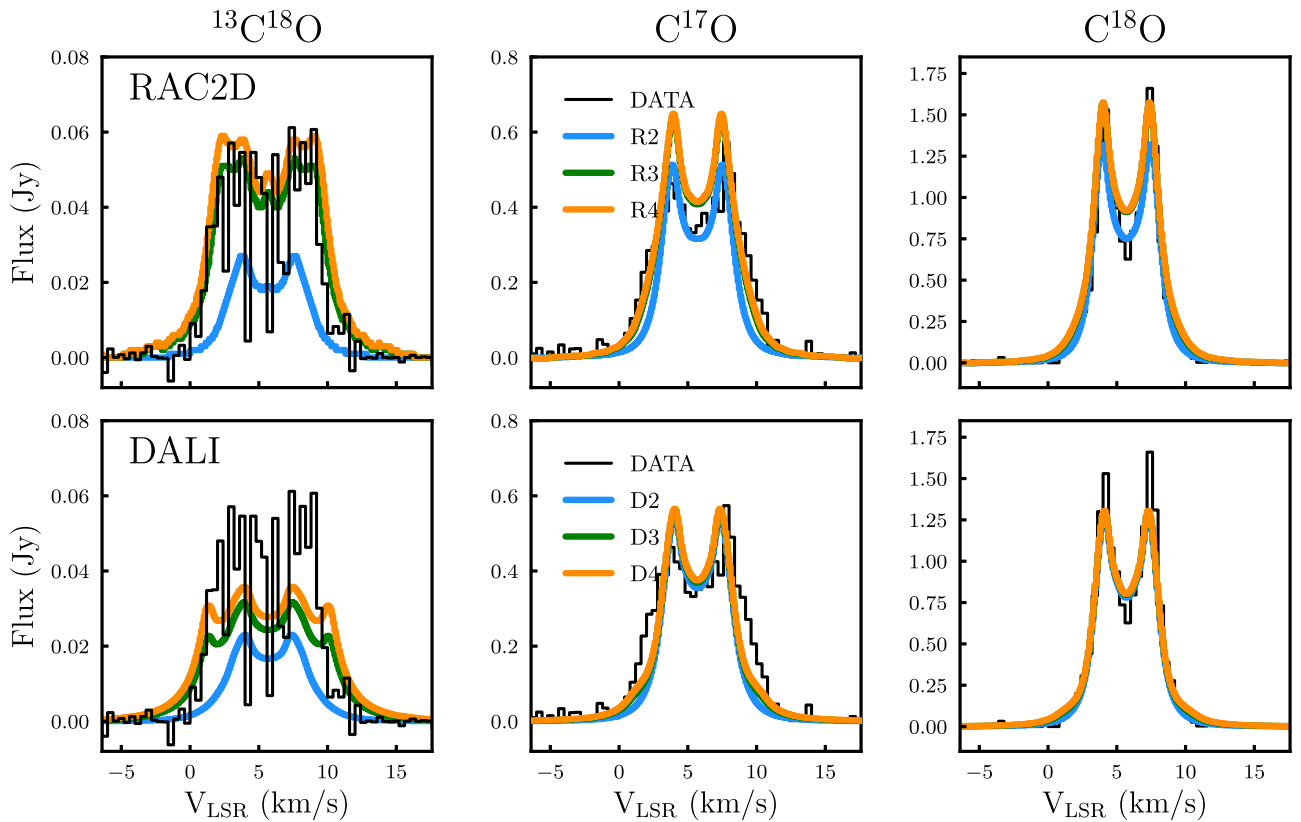**Figure 1.** C/H profiles used in the RAC2D and DALI models.

Figure 2. Comparison of RAC2D and DALI model spectra with observations. The best-fit models are the R3-4 and D3-4 models, which require a C/H ratio $\geqslant$ the stellar ratio inside the CO snowline.

4. Results

4.1. Models versus Observations

The model line spectra and integrated fluxes are shown in Figure 2 and Table 1. RAC2D and DALI models show consistent results, typically with less than 15% differences in line fluxes.

R1 and D1 models have a uniform ISM level of C/H ratio across the whole disk. These models overproduce line fluxes by a factor of ∼3 compared with observations. R2 and D2 models are uniformly depleted disk models (0.1× ISM C/H ratio);

these models match the integrated fluxes of $C^{18}O$ and $C^{17}O$ (2−1) observations. The model $C^{18}O$ line profiles also match well with observations, but $C^{17}O$ models are slightly narrower than the observations. This is most likely the result of hyperfine line splitting in the $C^{17}O$ (2−1) transition, which is not fully implemented in our ray-tracing code (Mangum & Shirley 2015). The R2 and D2 models underpredict the $^{13}C^{18}O$ (2−1) line flux by a factor of 2.4, and the model line profiles have an FWHM of only ∼6 km s⁻¹, which is much narrower than the observed FWHM of ∼10 km s⁻¹. This strongly hints that the $^{13}C^{18}O$ line emission originates from

velocities consistent with the inner ∼70 au; i.e., inside the CO snowline.

The R3-4 and D3-4 models represent distributions with an 1–2× ISM level of C/H ratio inside the CO snowline and a depleted C/H ratio gas of outer region. These models provide the best overall match to observations, and only these can match the observed $^{13}C^{18}O$ (2−1) line flux and the general profile. We note that these models over produce the line intensities at high-velocity channels that are $\geqslant 5$ km s^{-1} offset from the stellar velocity. One possible solution is that the C/H ratio inside ∼40 au is lower than the ISM level. However, the existing observations do not have sufficient signal-to-noise ratio or spatial resolution to constrain the detailed C/H profile inside 40 au.

4.2. Result Robustness

The HD 163296 disk is known to have substructures (e.g., gaps/rings) in its 1.3 mm continuum emission (Isella et al. 2016; Zhang et al. 2016). To test the effects of substructures in the continuum, we run additional models that include dust substructures and find that these do not change our conclusion.

All of our constraints on the C/H ratio in disk depend on the total disk mass. In Table 1, we show that our model HD (1−0) line fluxes are consistent or slightly overproduce the upper limit reported by Kama et al. (2020). This suggests that the total disk gas mass (0.14 $M_\odot$) in our models is an upper limit. Therefore, our estimation of the excess of C/H inside the CO snowline is a robust lower limit and the actual C/H can be even higher.

We note that there is a detection of $^{13}C^{17}O$ (3−2) line in the HD 163296 disk with the match-filter method (Booth et al. 2019). Although the line flux is uncertain, the detection suggests a high column of CO gas inside the CO snowline, which is consistent with our results.

In short, we find that in the HD 163296 protoplanetary disk: (1) the gas between 40 and 70 au has a C/H ratio of 1–2× the ISM value; (2) the gas outside 70 au has a C/H ratio of 0.1 × ISM value.

5. Discussion

The stellar carbon abundance represents the total amount of carbon available in the bulk materials of protoplanetary disks. Here we compare our results to the carbon abundance of the HD 163296 star. Its stellar C/H ratio is measured as $1.5^{+1.2}_{-0.7} \times 10^{-4}$ (Folsom et al. 2012; Jermyn & Kama 2018), which is about half of that in the Sun ($2.7^{+0.3}_{-0.3} \times 10^{-4}$; Asplund et al. 2009). Therefore, the HD 163296 system started with relatively carbon-poor materials than the ISM.

5.1. Fraction of Carbon in CO

Our C/H constraint is essentially a CO/H ratio, as our chemical models have $\geqslant 90\%$ of carbon in CO and the $^{13}C^{18}O$ (2−1) line spectrum does not sensitive to the region inside the CO_2 snowline (<40 au). Therefore, we discuss to what fraction CO can take up the total carbon budget. For reference points, we use carbon budgets measured in ISM, molecular clouds, protostellar cores, and solar system objects.

In the ISM, 50% of the cosmic carbon is locked in refractory grain materials (Draine 2003). More recently, Mishra & Li (2015) studied the abundance of carbon grains using the ultraviolet (UV) extinction along 16 Galactic sightlines. They found refractory carbon grains, on average, take 50% of the

total carbon budget, varying between 25% and 75% in their sample. These refractory materials are expected to survive from ISM to protoplanetary disks, because abundant carbon-rich grains are found in in-situ collections of dust in the coma of comet Halley and 67P/Churyumov (Jessberger et al. 1988; Bardyn et al. 2017). Theoretical studies also suggest that the processing of carbon grains is inefficient in protoplanetary disks (Anderson et al. 2017; Klarmann et al. 2018). Further, our own thermal models suggest that the refractory carbon grain destruction zone will lie interior to 1 au. We note that the bulk carbon abundance in chondrites is significantly lower than that of comets (e.g., Bergin et al. 2015); this likely requires refractory carbon grain destruction in the inner solar system that would release carbon to the gas. However, chondrites likely formed inside a few au and thus their compositions do not represent that of the radial region of >20 au that we study here.

For volatile carbon-materials, measurements of comets and protostellar cores provide the best constraints. Pontoppidan (2006) studied ice absorption features toward five young stellar sources in the Oph-F core and reported CO-to-CO_2 abundance ratios varying between 0.48 and 3. In a much larger sample, Öberg et al. (2011a) studied 63 young stellar objects. They found the combination of CO and CO_2 dominate the carbon budgets in ice species—on average, these two take 87% of the total carbon in ice species in low-mass stellar objects. The medium CO-to-CO_2 ratio is unity, and for most of the low-mass sources, the ratio varies between 0.4 and 2.5. Measurements of comets show similar CO-to-CO_2 ratios (Mumma & Charnley 2011). All these studies suggest that CO only takes a fraction of the total carbon budget in protoplanetary disks.

To evaluate the significance of the CO excess in the HD 163296 disk, we compare our constraint of CO abundance with two cases of CO fraction in the carbon budget. The first case is based on the average composition of the major carbon species discussed above. In this case, refractory carbon grains, CO_2, and CO take 50%, 25%, and 25% of the total stellar carbon budget, respectively. We note that including other minor carbon species, such as CH_4 and CH_3OH, will make the CO fraction even lower. For the second case, we consider a case that maximizes the carbon fraction in CO. We adopt the lowest carbon grain fraction of 25% found in diffuse ISM (Mishra & Li 2015), and a high CO-to-CO_2 abundance ratio of 3 (Pontoppidan 2006; Öberg et al. 2011a). Here refractory carbon grains, CO_2, and CO take 25%, 18.75%, and 56.25% of the total stellar carbon budget.

In Figure 3, we compare the CO fractions in these two cases with the CO abundance requirement of the inner 70 au of the HD 163296 disk. Compared with the best estimation of the stellar carbon abundance of 1.5×10^{-4}, our constraint of the CO abundance inside 70 au exceeds the expected value e by a factor of 4–8 in the case of the ISM average composition. In the case of the maximal CO fraction, the observational CO abundance is a factor of 1.8–3.6 higher than the expected abundance. However, we note that in the maximal CO fraction case, the lower limit of observational CO abundance inside 70 au is still consistent with the upper limit of the stellar carbon abundance. In summary, although we cannot completely rule out the possibility of a normal C/H ratio in the gas inside 70 au, our results suggest that the gas inside 70 au region of HD 163296 disk likely has an elevated C/H ratio that exceeds the expected value by a factor of 1.8–8.
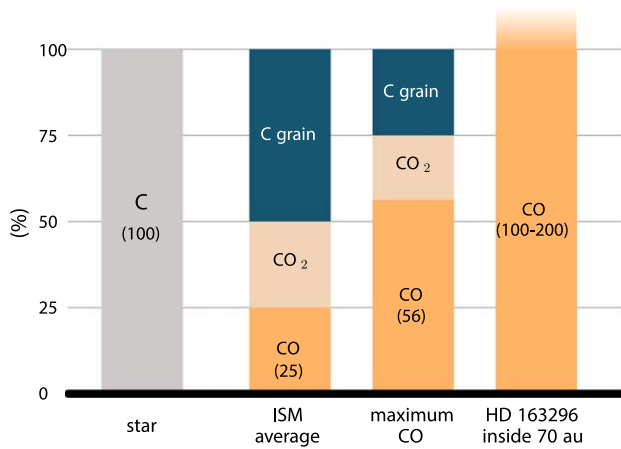
Figure 3. Comparison between the expected CO abundance with the observed CO abundance inside 70 au of the HD 163296 disk. The ISM average case represents average ratios of refractory carbon grains, CO_2, and CO seen in ISM, protostellar cores, and comets. The maximum CO case shows the highest fraction of carbon in CO, by adopting lower limits of other major carbon species.

5.2. Excess C/H as a Test of Pebble Drift Models

Our results suggest the gas inside 70 au of the HD 163296 disk has an elevated C/H ratio. Here we discuss the implication of this result in the context of the pebble accretion framework.

The mass flux of pebble drifting from the outer to the inner disk is a crucial parameter of the pebble accretion models. Here we do an order of magnitude estimation on the pebble mass flux in the HD 163296 disk. To increase the CO/H_2 ratio in the gas inside 70 au by a factor of 1.8–8, it requires an increase of the solid mass initially inside the 70 au region by the same factor, with a supply of CO-ice coated grains from the outer disk. In our HD 163296 model, this requires that 150–600 $M_\oplus$ of pebbles drift into the inner 70 au region within the disk lifetime. Given the age of the disk is estimated to be 5–10 Myr, this leads to a pebble mass flux of $\sim$15–60 $M_\oplus\,\mathrm{Myr}^{-1}$. This mass flux is comparable to the $\sim$95 $M_\oplus\,\mathrm{Myr}^{-1}$ derived from the analytical pebble drifting model of Lambrechts & Johansen (2014).

An elevated C/H gas ratio inside the CO snowline has long been predicted by models that include dust drift (Cuzzi & Zahnle 2004). More comprehensive simulations consider icy pebble formation, settling, and drifting with CO sublimation in a global disk setup (Booth et al. 2017; Stammler et al. 2017; Krijt et al. 2018). In general, these models predict the C/H gas ratio inside the CO snowline can be elevated to 1–10 times of the initial ratio, while the detailed radial distribution depends on various parameters, including viscosity, diffusion rate, and disk sizes. Although our data cannot constrain the detailed radial profile of the C/H ratio inside the CO snowline, we find that the gas inside $\sim$40 au might have a lower C/H ratio than the gas between 40 and 70 au, which is consistent with model predictions that the elevated C/H ratio is most prominent in region just inside the CO snowline.

To make a more quantitative comparison, in Figure 4 we compare our best-fit models with predictions of Krijt et al. (2018). Krijt et al. (2018) provides the only two-dimensional simulation that included the depletion of CO gas in the warm molecular layer outside the mid-plane CO snowline, which gives the closest theoretical comparison to our constraints on the C/H ratio in gas phase. Even the Krijt et al. (2018) models
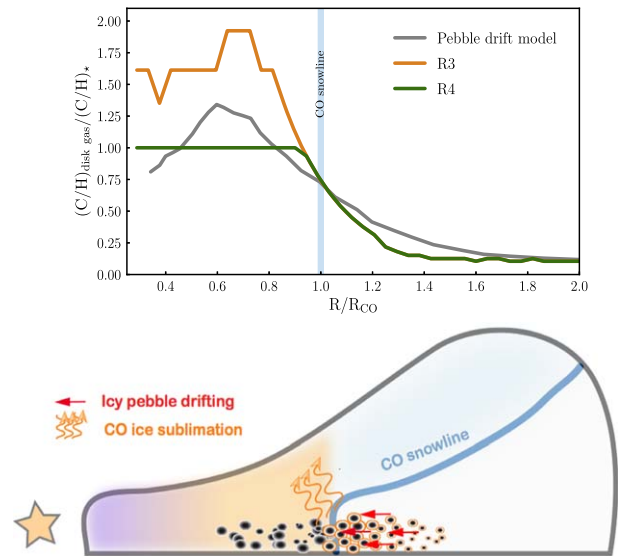
Figure 4. Top: comparison of our best-fit models with pebble drift simulations from Krijt et al. (2018). To rescale the CO/H_2 ratio from Krijt et al. (2018), we take the maximum abundance that 56% of carbon in CO (see the discussion in Section 5.1). Bottom: an illustrative figure that the disk gas in the CO snowline is enriched in C/H by ice pebble drift.

were for a generic disk; our best-fit models match the general profile within a factor of two.

However, we do not have sufficient spatial resolution or signal-to-noise ratio to constrain the detailed radial profile of the C/H ratio inside the CO snowline. Higher spatial resolution Atacama Large Millimeter/submillimeter Array (ALMA) images would be necessary to accurately constrain the elevated C/H ratio and quantitatively test current pebble drift simulations.

5.3. C/H and C/O Ratios as an Indicator of Planet Formation Location and History

The chemical composition of a giant planet depends on the relative amounts of disk gas and solids accreted during its formation, the compositions of which in turn depend on time and location. On top of that, planetesimal delivery and core-envelope mixing can further alter the atmospheric composition.

Given the complexity of the formation processes, it is challenging to uniquely attribute an elemental ratio in a planetary atmosphere to a single process. For example, a superstellar C/H atmosphere can be produced by accreting C/H-enriched disk gas, planetesimal contamination, or core erosion. Similarly, a C/O ratio of unity can be the product of accreting gas between the CO_2 and CO snowlines, or from the CO-enriched gas due to pebble drift into the CO snowline. The combination of several elemental ratios can be more constrictive. Öberg & Bergin (2016) and Booth et al. (2017) proposed that if a giant planet atmosphere has both a superstellar C/H and a C/O ratio $\sim$1, it is a unique indicator of a planetary atmosphere formed from gas enriched by ice pebble drift into the CO snowline.

It is also of particular interest to look at the case of the HD 163296 disk, as its abundant substructures suggest ongoing planet formation in the disk. Recent gas kinematic studies revealed signatures of gas flows into locations of three gaps opened by three giant planets in the HD 163296 disk (Teague et al. 2018, 2019). All three accreting planets are located

outside the CO snowline, where we find the C/H ratio in the gas phase is only $0.1\times$ stellar value. If these planets are still accreting a significant amount of their atmospheres, the high depletion C/H gas may leave a low C/H ratio in their final planetary atmospheres. Inside the CO snowline, the disk shows two additional gaps at 10 and 48 au in its 1.3 mm continuum image, which are characterized as gaps opened by Jupiter-mass planets (Zhang et al. 2018). Existing CO gas observations do not have sufficient resolution to show if gas also flows into these inner gaps. But if these planets are also accreting, the C/H ratio in their atmospheres would be an order of magnitude higher than these planets accreting atmospheres from the gas outside the CO snowline. Although highly speculative, the HD 163296 disk hints at the possibility that giant planets formed inside or outside of the CO snowline may carry distinctive C/H ratios in their atmospheres as a birthmark.

6. Summary

We report the first detection of excess C/H in the gas of a protoplanetary disk. In the HD 163296 disk, we find its gas just inside the CO snowline ($\sim$70 au) has a C/H ratio of 1.4–2.8×10^{-4}, which is 1–2$\times$ of the stellar C/H ratio of $1.5^{+1.2}_{-0.7} \times 10^{-4}$. This gas C/H inside 70 au is significantly higher than the expected ratio, as only 25%–60% of the stellar carbon budget should be in gas at these radii. Although existing observations cannot completely rule out the case of a normal C/H ratio inside 70 au, the most probable solution is an elevated C/H ratio of 1.8–8 times higher than the expected ratio. The C/H enriched gas is consistent with predictions of a large amount of icy pebble drift across the CO snowline.

Facility: NOEMA(PolyFix).

Software: RAC2D (Du & Bergin 2014), DALI (Bruderer et al. 2012; Bruderer 2013), GILDAS,[3] astropy (Astropy Collaboration et al. 2013).

ORCID iDs

Ke Zhang ⬤ https://orcid.org/0000-0002-0661-7517
Arthur D. Bosman ⬤ https://orcid.org/0000-0003-4001-3589
Edwin A. Bergin ⬤ https://orcid.org/0000-0003-4179-6394

References

Anderson, D. E., Bergin, E. A., Blake, G. A., et al. 2017, ApJ, 845, 13
Asplund, M., Grevesse, N., Sauval, A. J., & Scott, P. 2009, ARA&A, 47, 481
Astropy Collaboration, Robitaille, T. P., Tollerud, E. J., et al. 2013, A&A, 558, A33
Atreya, S. K., Wong, A. S., Baines, K. H., Wong, M. H., & Owen, T. C. 2005, P&SS, 53, 498
Bardyn, A., Baklouti, D., Cottin, H., et al. 2017, MNRAS, 469, S712
Bergin, E. A., Blake, G. A., Ciesla, F., Hirschmann, M. M., & Li, J. 2015, PNAS, 112, 8965
Bergin, E. A., Du, F., Cleeves, L. I., et al. 2016, ApJ, 831, 101
Booth, A. S., Walsh, C., Ilee, J. D., et al. 2019, ApJL, 882, L31
Booth, R. A., Clarke, C. J., Madhusudhan, N., & Ilee, J. D. 2017, MNRAS, 469, 3994
Bosman, A. D., Walsh, C., & van Dishoeck, E. F. 2018, A&A, 618, A182
Brewer, J. M., Fischer, D. A., & Madhusudhan, N. 2017, AJ, 153, 83
Brogi, M., de Kok, R. J., Birkby, J. L., Schwarz, H., & Snellen, I. A. G. 2014, A&A, 565, A124
Bruderer, S. 2013, A&A, 559, 46
Bruderer, S., van Dishoeck, E. F., Doty, S. D., & Herczeg, G. J. 2012, A&A, 541, A91
Ciesla, F. J., & Cuzzi, J. N. 2006, Icar, 181, 178
Cleeves, L. I., Adams, F. C., & Bergin, E. A. 2013, ApJ, 772, 5
Cridland, A. J., Pudritz, R. E., & Alessi, M. 2016, MNRAS, 461, 3274
Cridland, A. J., van Dishoeck, E. F., Alessi, M., & Pudritz, R. E. 2019, A&A, 632, A63
Cuzzi, J. N., & Zahnle, K. J. 2004, ApJ, 614, 490
Draine, B. T. 2003, ApJ, 598, 1017
Du, F., & Bergin, E. A. 2014, ApJ, 792, 2
Eistrup, C., Walsh, C., & van Dishoeck, E. F. 2016, A&A, 595, A83
Folsom, C. P., Bagnulo, S., Wade, G. A., et al. 2012, MNRAS, 422, 2072
Fortney, J. J., Marley, M. S., Saumon, D., & Lodders, K. 2008, ApJ, 683, 1104
Gail, H.-P., & Trieloff, M. 2017, A&A, 606, A16
Isella, A., Guidi, G., Testi, L., et al. 2016, PhRvL, 117, 251101
Jermyn, A. S., & Kama, M. 2018, MNRAS, 476, 4418
Jessberger, E. K., Christoforidis, A., & Kissel, J. 1988, Natur, 332, 691
Kama, M., Trapman, L., Fedele, D., et al. 2020, A&A, 634, A88
Klarmann, L., Ormel, C. W., & Dominik, C. 2018, A&A, 618, L1
Krijt, S., Schwarz, K. R., Bergin, E. A., & Ciesla, F. J. 2018, ApJ, 864, 78
Lambrechts, M., & Johansen, A. 2014, A&A, 572, A107
Lavie, B., Mendonça, J. M., Mordasini, C., et al. 2017, AJ, 154, 91
Lee, J.-M., Heng, K., & Irwin, P. G. J. 2013, ApJ, 778, 97
Line, M. R., Knutson, H., Wolf, A. S., & Yung, Y. L. 2014, ApJ, 783, 70
Madhusudhan, N. 2012, ApJ, 758, 36
Madhusudhan, N. 2019, ARA&A, 57, 617
Madhusudhan, N., & Seager, S. 2011, ApJ, 729, 41
Mangum, J. G., & Shirley, Y. L. 2015, PASP, 127, 266
Mishra, A., & Li, A. 2015, ApJ, 809, 120
Moses, J. I., Madhusudhan, N., Visscher, C., & Freedman, R. S. 2013, ApJ, 763, 25
Mumma, M. J., & Charnley, S. B. 2011, ARA&A, 49, 471
Öberg, K. I., & Bergin, E. A. 2016, ApJL, 831, L19
Öberg, K. I., Boogert, A. C. A., Pontoppidan, K. M., et al. 2011a, ApJ, 740, 109
Öberg, K. I., Murray-Clay, R., & Bergin, E. A. 2011b, ApJL, 743, L16
Owen, T., Mahaffy, P., Niemann, H. B., et al. 1999, Natur, 402, 269
Pollack, J. B., Hollenbach, D., Beckwith, S., et al. 1994, ApJ, 421, 615
Pollack, J. B., Hubickyj, O., Bodenheimer, P., et al. 1996, Icar, 124, 62
Pontoppidan, K. M. 2006, A&A, 453, L47
Qi, C., Öberg, K. I., Andrews, S. M., et al. 2015, ApJ, 813, 128
Rosenfeld, K. A., Andrews, S. M., Hughes, A. M., Wilner, D. J., & Qi, C. 2013, ApJ, 774, 16
Schwarz, K. R., Bergin, E. A., Cleeves, L. I., et al. 2018, ApJ, 856, 85
Stammler, S. M., Birnstiel, T., Panić, O., Dullemond, C. P., & Dominik, C. 2017, A&A, 600, A140
Teague, R., Bae, J., & Bergin, E. A. 2019, Natur, 574, 378
Teague, R., Bae, J., Bergin, E. A., Birnstiel, T., & Foreman-Mackey, D. 2018, ApJL, 860, L12
Tilling, I., Woitke, P., Meeus, G., et al. 2012, A&A, 538, A20
Williams, J. P., & Best, W. M. J. 2014, ApJ, 788, 59
Wilson, T. L. 1999, RPPh, 62, 143
Zhang, K., Bergin, E. A., Blake, G. A., et al. 2016, ApJL, 818, L16
Zhang, K., Bergin, E. A., Schwarz, K., Krijt, S., & Ciesla, F. 2019, ApJ, 883, 98
Zhang, S., Zhu, Z., Huang, J., et al. 2018, ApJL, 869, L47

---

[3] See http://www.iram.fr/IRAMFR/GILDAS for more information about the GILDAS softwares.